Behavior of Horizontally Curved I-Girders during Lifting

Jason C. Stith[1]; Todd A. Helwig, M.ASCE[2]; Eric B. Williamson, M.ASCE[3]; Karl H. Frank, M.ASCE[4]; Michael D. Engelhardt, M.ASCE[5]; Andrew C. Schuh[6]; Jamie F. Farris[7]; and Brian J. Petruzzi[8]

Abstract: Several stages of performance need to be considered during the design of curved I-girders, including both the construction stage and the in-service conditions. Girder stability during the early stages of construction can be difficult to assess because the girders, at times, have little or no bracing present. One stage when there is no bracing present occurs when the girders are picked up from the ground or transport trucks by cranes and lifted into place. To better understand girder response during this critical stage, field studies were conducted on horizontally curved I-girders to measure rotations and stresses during the lifting process. This paper provides details of a semianalytical solution to predict the buckling and deformational responses of straight and curved girder segments during lifting. The deformations can be compared with rotational limits that were established to minimize problems with making connections to previously erected girder segments. The total rotational deformations of a horizontally curved girder result from two distinct components: (1) rigid-body rotation and (2) rotation caused by the girder cross-sectional twist owing to torsion from the girder's self-weight. A spreadsheet design tool, *UT Lift*, was developed to provide critical information for evaluating the rotational behavior of a horizontally curved I-girder during lifting and to estimate its lateral-torsional buckling capacity. An example of *UT Lift*'s capabilities is presented along with background information on its development. Recommendations are given for safely lifting and erecting horizontally curved steel I-girders. **DOI: 10.1061/(ASCE)ST.1943-541X.0000674.**

CE Database subject headings: Steel structures; Girders; Curvature; Computer software.

Author keywords: Steel structures; Curved girders; Software.

Introduction

The design of curved I-girders requires an evaluation of the girder response at several potentially critical stages during construction and while in service. Girder stability during the early stages of construction can be difficult to assess because little or no bracing may be present. For example, generally no bracing is provided when a single girder segment is picked up from the ground or transport trucks by cranes and lifted into place. The stability of a steel I-girder is primarily a function of the geometry of the girder segment and the location of the lifting points. The sophistication and method of analysis performed by an erection engineer to locate girder lift points varies widely among contractors. Due to uncertainties in girder stability, as well as the wide range of analysis methods used to check erection sequencing, the Texas Department of Transportation (TxDOT) funded a research project to investigate the behavior of straight and curved girder systems throughout construction. Preferred practices by TxDOT (2007) employ recommended girder proportions that are twice as large as the minimum specified values in AASHTO (2010). One of the goals of the investigation was the development of recommendations for girder proportions that allow for safe and economical construction. In addition, the study focused on the creation of guidelines for the evaluation of girder stability during early construction stages. The research included field monitoring, parametric finite-element analyses, and the development of user-friendly finite-element software to serve as a tool for designers and erectors. While this research project was specifically focused on bridge girders, the results presented in this paper are applicable to a variety of girder erection scenarios encountered in practice. For example, there are a number of applications in the building industry that may necessitate horizontally curved girders. One such application may be curved spandrel girders that are required based on architectural features. Another likely application can occur in stadium roofing systems that often incorporate circular compression rings composed of several curved beams.

Field studies were conducted to measure the rotation and stresses of curved I-girders throughout the erection process. The collected data provide valuable information for understanding the fundamental behavior of girders during erection and further provide validation of three-dimensional (3D) finite-element models used to conduct parametric investigations that extend the range of possible system geometries. This paper includes details of a semianalytical solution to predict the behavior of girder segments during lifting, allowing engineers and erectors the ability to evaluate the

[1]Civil Engineer, Michael Baker Jr., Inc., 9750 Ormsby Station Rd., Louisville, KY 40223 (corresponding author). E-mail: Jason.Stith@mbakercorp.com

[2]Associate Professor, Univ. of Texas, Austin, TX 78712. E-mail: thelwig@mail.utexas.edu

[3]Professor, Univ. of Texas, Austin, TX 78712. E-mail: ewilliamson@mail.utexas.edu

[4]Chief Engineer, Hirschfeld Industries, 112 W 29th St., San Angelo, TX 76903. E-mail: karl.frank@hirschfeld.com

[5]Professor, Univ. of Texas,. Austin, TX 78712. E-mail: mde@mail.utexas.edu

[6]Structural Engineer, Mustang Engineering, Inc., 16001 Park Ten Place, Houston, TX 77084. E-mail: andrew.schuh@mustangeng.com

[7]Bridge Design Engineer, Texas Dept. of Transportation, Bridge Division, 125 East 11th St., Austin, TX 78701. E-mail: jfarris@dot.state.tx.us

[8]Structural Engineer, Weidlinger Associates, Inc., 1825 K St. NW #350, Washington, DC 20006. E-mail: petruzzi@wai.com

Note. This manuscript was submitted on November 30, 2011; approved on June 5, 2012; published online on August 11, 2012. Discussion period open until September 1, 2013; separate discussions must be submitted for individual papers. This paper is part of the ***Journal of Structural Engineering***, Vol. 139, No. 4, April 1, 2013. ©ASCE, ISSN 0733-9445/2013/4-481–490/$25.00.

vulnerability of the lifted segment to construction issues such as excess rotation, cross-sectional yielding, and girder buckling. Based on feedback from a nationwide survey of contractors, inspectors, and engineers that specialize in curved steel I-girder systems, girder rotation during lifting was found to be important for ensuring proper connection fit-up of air splices (Farris 2008). The total rotational deformations of a curved I-girder can be divided into two distinct components: (1) rigid-body rotation and (2) torsional deformations of the girder cross section caused by the girder's self-weight acting eccentrically to the lifting points. A spreadsheet design tool, *UT Lift*, was developed to provide critical information for evaluating the rotational behavior of a girder segment during lifting and for estimating its lateral-torsional buckling capacity. The program is available for free from the University of Texas at Austin Ferguson Structural Engineering Laboratory website (http://fsel.engr.utexas.edu/software/). In this paper, background information on the development of the *UT Lift* program is provided, along with an example demonstrating the program features and capabilities. Based on the findings from this research, recommendations are made for safely lifting and erecting horizontally curved steel I-girders.

Background

The behavior of curved girder systems can be difficult to assess because of the large torsional moments that result from the geometry of the girders. The curved geometry creates numerous challenges for engineers and contractors, including girder transportation, staging, lifting, and the prediction of stresses. Although there are a few field studies on the behavior of curved I-girders during construction (Beal and Kissane 1971a, b,1972; Galambos et al. 2000; and Linzell et al. 2004), the authors are not aware of any studies on the behavior of the girders during erection when no bracing is present. The behavior during lifting is a stage of response that is not well understood from the perspectives of stability and deformation. Davidson (1996) modeled curved I-girders using finite-element models and determined critical lift points for prismatic girders, noting that excessive deformations and rotations can be problematic during lifting. Mast (1989) suggested a set of equations to determine the factor of safety for lifting long precast concrete beams. Mast's equations apply to prismatic girders with some initial imperfection, and they include a factor for lateral stiffness and for initial rigid-body rotation (roll angle) of the beam being analyzed.

The field tests that were performed as part of the study discussed in this paper were conducted on a curved steel I-girder during lifting at the Hirschfeld Steel Fabrication Plant in San Angelo, Texas, as reported by Stith et al. (2012) and Schuh (2008). The results of the field tests confirmed that curved steel I-girders during lifting are subject to both rigid-body rotations and cross-sectional twist. Additionally, a significant finding from the collected test data is that the warping stresses can be of the same order of magnitude as the strong-axis bending stresses. Thus analyses of curved steel I-girders during lifting should accurately account for the stresses and deformations that result during this critical stage of performance.

Lifting of Curved I-Girders

Three-Dimensional Parametric Study

Data gathered during the field measurements provided valuable information for validating the modeling techniques and assumptions used to analyze curved I-girders during lifting. Because of the limited girder support that exists during lifting, proper modeling is paramount to obtaining a good understanding of behavior. For this research, parametric analyses were conducted using a 3D finite-element model developed in *ANSYS*. The model employed eight-noded shell elements for the girder flanges, web, and stiffeners. Fig. 1 shows the beam clamp and associated hardware on the crane used to lift the girders. The lifting hardware was modeled using truss elements positioned along a line of action between the lift points and the clamp support mechanism. A flexible lateral spring was attached to the bottom flange of the girders to properly restrain the model and to prevent rotation about the lift points. Inclusion of the spring in the model was necessary to account for the frictional forces in the lifting apparatus. The spring stiffness used in the model was 0.05 k/in. (87.6 N/mm) and was calibrated from the rotational measurements obtained from the field test. In addition to ensuring equilibrium of the girder segment, the spring also served the purpose of providing some resistance to the girders to aide in computational convergence. Other solutions to this numerical problem exist, such as including a rotational spring at the lift clamp support. However, the chosen method provided an efficient solution, allowing the selection of a spring constant that could be readily specified using data collected during the field studies.

Schuh (2008) and Farris (2008) showed that the stability of girder segments during lifting is significantly affected by the boundary conditions of the girders. Fig. 2 is a schematic of the girder system that was modeled by Schuh and Farris. The figure shows the elevation of the girder in which the lift-point location was varied from the end of the girder by a distance a. For a straight prismatic girder of length L, the lateral torsional buckling capacity can be maximized by lifting the girder symmetrically at a distance $a = 0.238L$ from the ends. For curved girder segments, however, it is also important to consider the deformational behavior of the girder. For curved prismatic segments, the girder twist from rigid-body rotation can be minimized if the girder is lifted symmetrically at a distance of $a = 0.211L$ from the ends. Eigenvalue buckling analyses were performed to investigate the stability of prismatic girders (Schuh 2008) as well as nonprismatic girders (Farris 2008) during lifting. Moment gradient factors (C_b) were developed to account for the variation in stability as a function of the lift locations, but it was observed that the radius of curvature did not significantly affect the

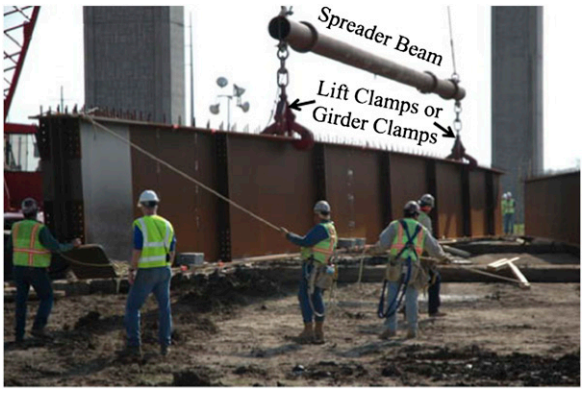

Fig. 1. Lifting of a curved I-girder with a spreader beam and lift clamps

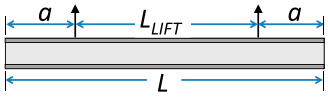

Fig. 2. Girder lifting schematic

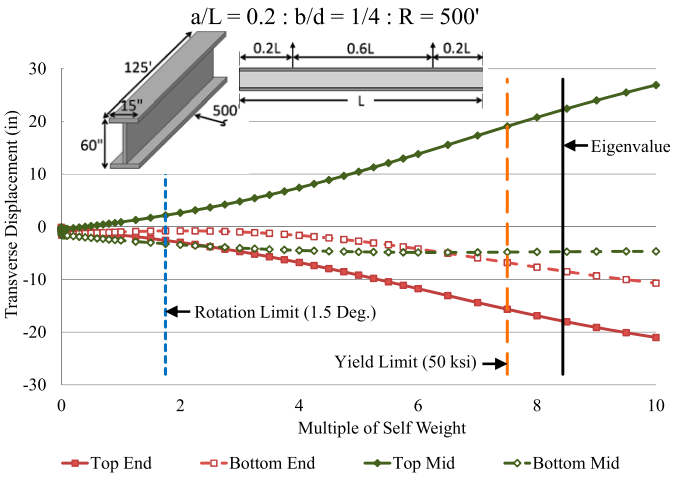

Fig. 3. Nonlinear analysis of transverse displacement versus multiple of self-weight: $R = 152.4$ m (500 ft)

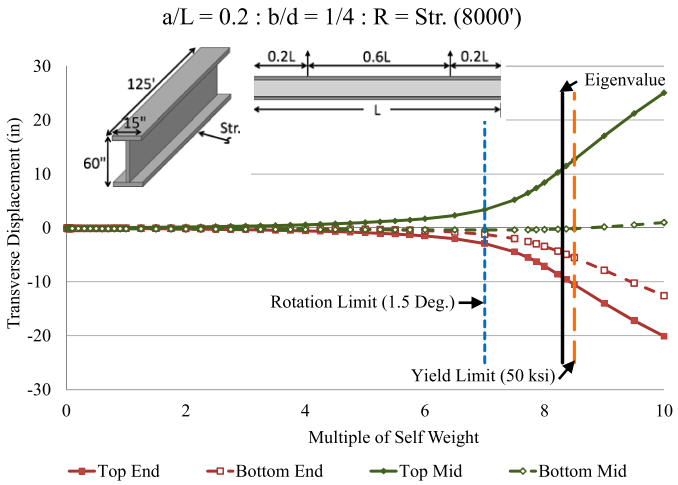

Fig. 4. Nonlinear analysis of transverse displacement versus multiple of self-weight: $R = 2{,}438.4$ m (8,000 ft)

predicted buckling capacity with an eigenvalue buckling analysis. Implicit in linear eigenvalue analyses is the assumption that displacements prior to buckling remain infinitesimal. This assumption is not valid for cases in which significant displacements occur prior to buckling, such as the case for highly curved girders. To model structural behavior properly under these conditions, a large-displacement nonlinear analysis must be performed. For horizontally curved I-girders, the curvature is similar to a large initial imperfection that results in significant deflection from the applied loading. This nonlinearity typically prevents the girder from reaching the predicted linearized eigenvalue buckling capacity.

Using the *ANSYS* analysis model (*ANSYS*) to study behavior for various girder geometries and lifting locations demonstrated that two limit states were critical: strength and serviceability. The strength limits should include buckling considerations in addition to stress limits. The stress limits should consider strong- and weak-axis bending stresses as well as warping stresses. For service levels of applied loading, a stress limit of 50% of F_y during construction was deemed to be reasonable in this study because such a limit usually will avoid problems with yielding from the combination of applied stresses and the initial residual stresses imposed during fabrication. The serviceability limits during erection should consider end rotation at the girder splice, and a limiting value of 1.5° is recommended. This serviceability limit was established from a nationwide survey conducted by Farris (2008). The serviceability limit state should account for the rigid-body rotation and the cross-sectional distortion resulting from torsion on the curved girder due to its self-weight.

The effect of horizontal curvature on the behavior of girders during lifting can be understood by comparing the deformational response of girders with different geometries. A girder with a radius of curvature R equal to 152.4 m (500 ft) was deemed highly curved in this study, whereas a radius of curvature greater than or equal to 2,438.4 m (8,000 ft) was deemed relatively straight. The variations in lateral displacement of the two flanges for girders with horizontal curvature at these two extremes are shown in Figs. 3 and 4. The lifting points for the girders were positioned at $a = 0.2L$ from the ends, which is close to the optimal locations to maximize strength ($0.238L$) and minimize rotation ($0.211L$) mentioned previously. The lateral flange displacements are graphed on the vertical axis, and the horizontal axis represents multiples of the girder self-weight. For lifting of girders, the only load acting is the girder self-weight. The deformations were determined from a large displacement analysis. In addition to the flange displacements, three limits are shown, representing serviceability (rotational limit of 1.5°) and strength limits [yield limit of 345 kPa (50 ksi) and the buckling load predicted from an eigenvalue buckling analysis]. The eigenvalue represents a multiplier to the applied load (i.e., the girder self-weight), which is the main reason the abscissa was selected as the multiple of the self-weight. The curved girder results shown in Fig. 3 indicate that the lines representing the top and bottom flange displacements bifurcate immediately. Physically, this indicates that the girder experiences significant twisting as soon as load is applied and continues to twist as the load is increased. The displacement at the eigenvalue buckling load level is in excess of 508 mm (20 in.). The straight girder results shown in Fig. 4 with an initial imperfection of $\sim L/500$ (L is the total length of the girder) remain relatively straight until they approach the eigenvalue buckling load. Large deformations occur near the eigenvalue limit, which indicates that the critical-load prediction is a reasonable approximation for the buckling capacity of straight girders. Thus, when the load on the straight girder nears the eigenvalue limit, the system becomes unstable, with large torsional deformations synonymous with the lateral-torsional buckling mode, which signifies failure. In both cases, and what is expected to be the most likely situation in practice, the rotational limit state controls the behavior during the lifting process, but the limit is reached at a much lower load level than the eigenvalue buckling load for the highly curved girder. A full explanation of the nonlinear lift study is presented by Petruzzi (2010).

Based on these observations, it is clear that a detailed understanding of the behavior of curved girders during lifting relies on accurate predictions of the rotational deformations that occur. As mentioned previously and verified with the data collected during the girder lift tests, girder rotations consist of two distinct components: (1) rigid-body rotation and (2) cross-sectional twist. The rigid-body rotation calculated in the next section is applicable to any circularly curved beam, prismatic or nonprismatic. The cross-sectional twist calculations are generally accurate for values of rigid-body rotation that can be reasonably expected to occur in practice.

Rotational Deformation of Curved I-Girders

Rigid-Body Rotation

Mast (1989) provided an equation to calculate the roll angle during lifting for a prestressed concrete I-girder with an initial imperfection.

J. Struct. Eng., 2013, 139(4): 481-490

While concrete I-girders are often prismatic, most steel I-girders are not. Because the basic concepts are the same, however, Mast's solution can be extended to the case of steel I-girders by recognizing that there is a line of support defined by a line through the lifting apparatus. The rigid-body rotation of a curved girder is caused by the center of gravity of the girder not being located collinearly with the line defined by the lifting locations. This eccentricity results in a system that has stored potential energy that will rotate the girder until the center of gravity is directly below the line of support, thereby minimizing the potential energy of the system. A schematic of this process is shown in Fig. 5. Calculating the location of the center of gravity for a curved I-girder becomes a critical step in determining the lifting behavior. The following equations can be used to determine the location of the center of gravity of a curved nonprismatic girder with (potentially) multiple cross sections and cross fames:

$$\overline{\theta} = \frac{R\sum_i^n W_i\left(\theta_i^2 - \theta_{i-1}^2\right)}{2} + \sum_j^m Wx_j\ \theta x_j \Big/ R\sum_i^n W_i(\theta_i - \theta_{i-1}) + \sum_j^m Wx_j \tag{1}$$

$$\overline{L} = \overline{\theta}R \tag{2}$$

$$\overline{D} = \frac{R^2\sum_i^n W_i\ [\sin(\theta_i - \overline{\theta}) - \sin(\theta_{i-1} - \overline{\theta})] + \left(R + \alpha\frac{s}{2}\right)\sum_j^m Wx_j \cos\left(\theta_j - \overline{\theta}\right)}{R\sum_i^n W_i(\theta_i - \theta_{i-1}) + \sum_j^m Wx_j} \tag{3}$$

where $\overline{\theta}$ = angular distance to the center of gravity of the girder, R = radius of curvature, W_i = weight per unit length of cross-section i, θ_i = internal angle from the beginning of the girder to the end of section i, Wx_j = weight of cross frame j, n = total number of different cross sections, m = total number of cross frames, θx_j = internal angle from the beginning of the girder to cross frame j, $\overline{L}$ = length along the girder to the center of gravity, $\overline{D}$ = radial distance to the center of gravity, s = spacing of the girder (assumed to be the width of the cross frame), and $\alpha = -1, 0, \text{or} 1$ depending on the cross-frame location.

The eccentricity of the center of gravity (CG) from the line of support e and the distance of the center of gravity below the line of support provide the necessary information to calculate the rotational angle, as depicted in Fig. 5 and given in Eq. (4). In this equation, $\overline{H}_{\text{C.G.}}$ is the weighted average for all cross-sectional $H_{\text{C.G.}}$ values along the length of the girder. As expected, the rigid-body rotation θ_{rigid} is not a function of the cross-sectional stiffness of the girder but rather only a function of the girder and lifting geometry

$$\theta_{\text{rigid}} = \tan^{-1}\left(\frac{e}{H + t_T + \overline{H}_{\text{C.G.}}}\right) \tag{4}$$

where H = distance from the line of support to the top of the girder, and t_T = top-flange thickness.

A result of this calculation is that there are an infinite number of lines that pass through the center of gravity and represent lines of support that prevent girder rotation. However, there is a unique solution to the problem if an additional constraint is applied. If a girder has lift locations equidistant (along a straight line) from the center of gravity, the reaction on each lift clamp will be equal, which will prevent girder rotation. The constraint of equal reactions is necessary in the most frequently used lifting systems shown in Fig. 1, where equal reactions are required for equilibrium of the spreader beam with a single crane. Therefore, by enforcing the constraint that the lifting forces at each lift point be equal, it is possible to compute these lifting locations as shown in Fig. 6 and indicated in the following equations:

$$\theta' = \cos^{-1}\left(\frac{\overline{D}}{R}\right) \tag{5}$$

$$\theta_{\text{Lift 1}} = \overline{\theta} - \theta' \tag{6}$$

$$L_{\text{Lift 1}} = R\theta_{\text{Lift 1}} \tag{7}$$

$$L_{\text{Lift 2}} = R\left(\theta_{\text{Lift 1}} + 2\theta'\right) \tag{8}$$

where θ' = angle from the first lift point to the center of gravity, $\theta_{\text{lift 1}}$ = angular distance from the beginning of the girder to the first lift point, $L_{\text{lift 1}}$ = length along the girder to the first lift point, and $L_{\text{lift 2}}$ = length along the girder to the second lift point. As a result of these conditions, the lifting location for a prismatic girder resulting in zero rigid-body rotation is computed to be $L_{\text{lift 1}}/L \approx 0.211$. This solution was confirmed from finite-element parametric studies using a 3D model (Stith 2010).

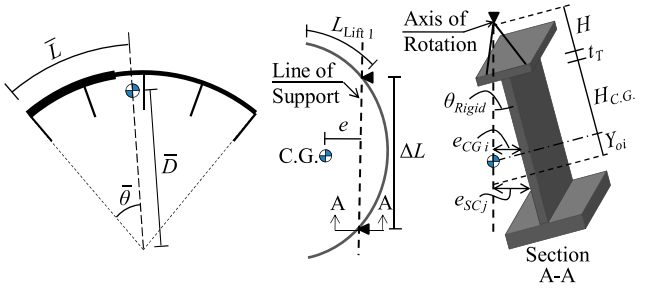

Fig. 5. Schematic of girder rotation and center of gravity location

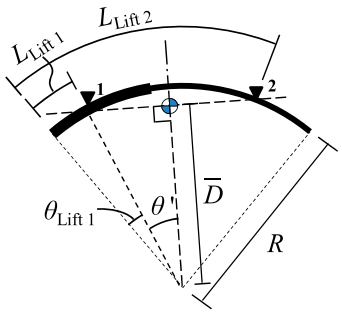

Fig. 6. Schematic of lift locations to prevent girder rotation

J. Struct. Eng., 2013, 139(4): 481-490

Cross-Sectional Twist

Unlike rigid-body rotation, which depends only on the girder and lifting geometry, cross-sectional twist is a function of both the girder torsional stiffness and the torsion distribution that is effectively applied by the girder's self-weight. Accounting for these effects presents two challenges when approaching the problem: (1) the I-girder shape is an open section that relies on both St. Venant and warping torsional stiffness, and (2) the applied torque is nonuniform along the length, for which an exact solution is not available. To overcome these challenges, a numerical approximation of the cross-sectional twist was proposed and adopted in this research. The closed-form solution of the rigid-body rotation can be readily computed with the procedure given in the preceding section. However, the numerical solution of rigid-body rotation within a 3D finite-element analysis, which is a necessary step in the overall process of capturing critical response phenomena such as warping, is computationally demanding. The demand is due to the iterative solution involving geometric nonlinearity in which convergence is ensured by the inclusion of a small restraint. Rather than carrying out such a finite-element analysis, an alternative approach is to calculate the rigid-body rotation analytically and then develop an algorithm that computes the resulting nodal locations in the deformed position. Once this deformed position is computed, a numerical solution procedure is used to determine twisting deformations. The numerical procedure uses a two-node, one-dimensional, C^1 continuous finite-element formulation for an open cross section with an applied nonuniform torsion derived by Mohareb and Nowzartash (2003) to linearly approximate the twist and the rate of change of twist. A displacement-based C^1 continuous finite element has the property that the primary variable (i.e., rotations) and the derivative of the primary variable are continuous at the boundary between two elements. The element employed in this research captured the necessary behavior as a one-dimensional linear element, allowing the girder's arc length to be modeled as a straight line. The general finite-element equation for this element is given by Eq. (9)

$$[K_e]\{\varphi\} = \{T_{eFE}\} + \{T\} \tag{9}$$

where $[K_e]$ = torsional stiffness matrix, $\{\varphi\}$ = nodal rotations, $\{T\}$ = nodal torsional moments, and the fixed-end torques $\{T_{eFE}\}$ are computed from Eq. (10)

$$\{T_{eFE}\} = \int_{z=0}^{z=l} \{N_i(z)\}t(z)dz \tag{10}$$

The formulation given by Mohareb and Nowzartash (2003) provides the torsional stiffness matrix $[K_e]$ and the shape functions $\{N_i(z)\}$, but it requires the applied distributed twisting moment $t(z)$ to be defined. This term can be computed as the derivative of the function that describes the variation in torsion evaluated at the integration point of an element. Previously, Stith et al. (2009) derived the torsion diagram equations (i.e., the variation in torsion) for a prismatic girder. However, many steel I-girders are nonprismatic, and additional equations for a nonprismatic girder were developed to represent this case.

Loads that do not pass through the shear center of a girder cross-section produce a torque on the member. It is therefore necessary to determine the eccentricity of the load from the cross-sectional shear center to determine the torque at a particular location along the girder. To derive the torsion diagram, an approach similar to the calculation of the bending-moment diagram is used. Equilibrium between the internal and external forces is established by taking a section through the girder. The external loads include the girder self-weight, the weight of the cross frames, and the lifting-clamp reactions. Unlike the moment diagram on a straight girder, the torsion diagram is computed on a two-dimensional (2D) girder curved in plan and thus is slightly more complicated. It is also important to note that the torsion diagram must be calculated on the rigidly rotated girder so that the resulting diagram produces zero net torque. Additionally, after the rigid-body rotation takes place, the center of gravity and shear center for any given cross section generally will not align vertically and thus will move perpendicularly to the line of support in plan, as shown in Figs. 7 and 8.

With the rigid-body rotation angle θ_{rigid} and the eccentricity between the center of gravity of the girder and the line of support e known, the eccentricity of the shear center at cross section j and the center of gravity for a given cross section i is given by Eqs. (11) and (12)

$$e_{\text{S.C.}j} = e\frac{(H + t_T + H_{\text{S.C.}j})}{(H + t_T + \overline{H}_{\text{C.G.}})} \tag{11}$$

$$e_{\text{C.G.}i} = e\frac{(H + t_T + H_{\text{C.G.}i})}{(H + t_T + \overline{H}_{\text{C.G.}})} \tag{12}$$

$$e_{YOj-i} = e_{\text{S.C.}j} - e_{\text{C.G.}i} \tag{13}$$

where $H_{\text{S.C.}j}$ = height of the shear center (SC) at cross section j and is equal to $H_{\text{C.G.}} + Y_{Oj}$, $e_{\text{S.C.}j}$ = eccentricity of the shear center at cross section j to the line of support, $e_{\text{C.G.}i}$ = eccentricity of the center of gravity at cross section i to the line of support, and e_{YOj-i} = eccentricity of the shear center at cross section j to center of gravity at cross section i.

Fig. 7 shows the centerline of the prerotated girder as the arc of girder support. The arc of girder shear center is the rotated position of the girder's shear center in plan view owing to the rigid-body rotation of the girder. The equations necessary to calculate the torque applied to the specified cross section x by the lift clamps are given subsequently. The torque effectively applied by both lifting clamps 1 and 2 are calculated the same way, but only the lifting clamp 1 equations are shown subsequently for conciseness. $R_{\text{lift 1}}$ is the reaction force at lifting clamp 1 calculated from an equilibrium analysis of this statically determinate system, and $T_{\text{lift 1}}$ is the

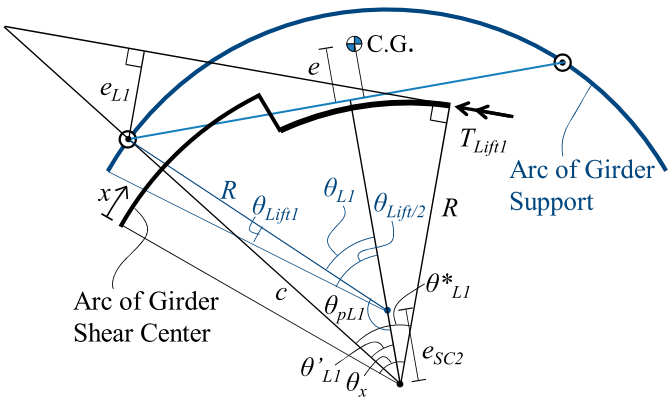

Fig. 7. Plan view schematic of lifted nonprismatic girder torque owing to Lift Clamp 1 at a point θ_x

J. Struct. Eng., 2013, 139(4): 481-490

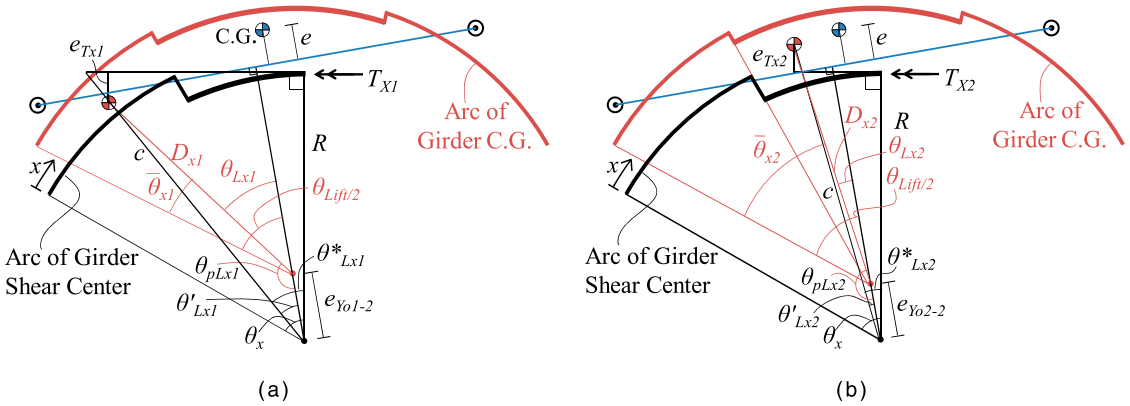

Fig. 8. Plan view schematic of lifted nonprismatic girder torque owing to self-weight of (a) Cross Section 1 and (b) Cross Section 2 at a point θ_x

resulting interior torque at x due to lifting clamp 1. Eqs. (14)–(21) provide the derivation necessary to calculate $T_{\text{lift 1}}$ given in Eq. (22), which is used in the subsequent analysis of the girder cross-sectional twist. All other variables used in Eqs. (14)–(21) are shown in Fig. 7

$$\theta_x = \frac{x}{R} \tag{14}$$

$$\theta_{\text{Lift}/2} = \frac{\theta_{\text{Lift 1}} + \theta_{\text{Lift 2}}}{2} \tag{15}$$

$$\theta_{L1} = \theta_{\text{Lift}/2} - \theta_{\text{Lift 1}} \tag{16}$$

$$\theta_{\pi L1} = \pi - \theta_{L1} \tag{17}$$

$$c = \sqrt{R^2 + e^2_{\text{S.C.}j} - 2R \times e_{\text{S.C.}j} \times \cos(\theta_{\pi L1})} \tag{18}$$

$$\theta'_{L1} = \sin^{-1}\left[\frac{R \times \sin(\theta_{\pi L1})}{c}\right] \tag{19}$$

$$\theta^*_{L1} = \theta_x + \left(\theta'_{L1} - \theta_{\text{Lift}/2}\right) \tag{20}$$

$$e_{L1} = \left[\frac{R}{\cos(\theta^*_{L1}) - c}\right]\cos(\theta^*_{L1}) \tag{21}$$

$$T_{\text{Lift 1}} = R_{\text{Lift 1}} \times e_{L1} \tag{22}$$

The next step is to calculate the resultant force effectively applied by the self-weight of the girder to the location of the cut x. The weight of the girder sections W_{xi} is calculated based on the dimensions of the cross section and the material density. The location of the centroid $(\overline{\theta}_{xi}, D_{xi})$ of each section can be calculated using Eqs. (1)–(3). With this information, Eqs. (23)–(28) can be used to calculate the torque from the girder self-weight for cross section j at the cut located on cross section i (T_{xi}). The results from Eqs. (22) and (29) are combined to give the torsion function shown in Eq. (30). Fig. 8 provides schematic diagrams of the method to calculate the eccentricities (1) between the girder's first cross section center of gravity and the tangent line at x and (2) between the girder's second cross section center of gravity and the tangent line at x. As a result of rigid-body rotation, both the center of gravity and the shear center will translate in plan as shown in Fig. 8. Nonprismatic girders require the

$$\theta_{Lxi} = \theta_{\text{Lift}/2} - \overline{\theta}_{xi} \tag{23}$$

$$\theta_{\pi Lxi} = \pi - \theta_{Lxi} \tag{24}$$

$$c = \sqrt{D^2_{xi} + e^2_{YOj-i} - 2D_{xi} \times e_{YOj-i} \times \cos(\theta_{\pi Lxi})} \tag{25}$$

$$\theta'_{Lxi} = \sin^{-1}\left[\frac{D_{xi} \times \sin(\theta_{\pi Lxi})}{c}\right] \tag{26}$$

$$\theta^*_{Lxi} = \theta_x + \left(\theta'_{Lxi} - \theta_{\text{Lift}/2}\right) \tag{27}$$

$$e_{Txi} = \left[\frac{D_{xi}}{\cos(\theta^*_{Lxi})} - c\right]\cos(\theta^*_{Lxi}) \tag{28}$$

$$T_{xi} = W_{xi} \times e_{Txi} \tag{29}$$

$$\Rightarrow T(x) = \sum T_{xi} - T_{\text{Lift 1}} - T_{\text{Lift 2}} \tag{30}$$

summation over all cross sections along the girder to the cut at x. All other variables used in Eqs. (23)–(28) are shown in Fig. 8.

Several graphic examples of torsion diagrams are provided in Stith, et al. (2009). The derivative of the torsional moment function at the integration points was computed using a linear five-point central-difference scheme because its quadratic approximation of the derivative provided increased accuracy over lower-order numerical procedures.

UT Lift Analysis Tool

The culmination of the research on the lifting of curved I-girders resulted in the development of the *UT Lift* analysis tool (an example analysis using this software is provided in the Appendix). The program is a spreadsheet-based tool that allows the user to input the girder properties such as number of cross sections, radius of curvature, cross-sectional properties, and cross-frame information. The program calculates the center of gravity and the ideal lift-point locations that result in no rigid-body rotation. The program also allows the user to specify the lift points based on erection hardware such as the specific crane spreader bar length. Based on the user-defined lift points, the program calculates the rigid-body rotation

using the analytical solution described previously. Girder twist resulting from the applied torque is also evaluated using a macro within the spreadsheet software that employs the Mohareb and Nowzartash (2003) element formulation described in the preceding section.

Stresses and Buckling Moments

The strong- and weak-axis bending displacements are modeled using a two-node beam element that neglects axial and torsional components. This formulation yields a two-node, four-degree-of-freedom element that is combined and uncoupled from the open-section torsion element, producing an element with a total of six degrees of freedom (displacement and rotation about the strong and weak axes as well as twist and change of twist about the longitudinal axis of the girder). The lift points apply a point torque, and it is desirable to report the deformations at the midpoint between lifting clamps. Thus the girder is divided into four segments: a segment from the beginning of the girder to the first lift point, two segments between the lift points, and a segment from the second lift point to the end of the girder. There are multiple elements per segment, but subdividing the girder into segments ensures that, in general, nodes are located at critical girder locations. The only strong- and weak-axis bending loads are due to the girder and cross-frame weights decomposed into components based on the calculated rigid-body rotation. Once the weak-axis displacements are calculated, a correction is made to the girder's center of gravity, and a new rigid-body rotation is calculated. However, the process is not iterative because the cross-sectional twist approximation is linear.

The output produced by *UT Lift* includes the cross-sectional stresses at the top and bottom flange tips, the total rotation at the ends and midway between the lift points, and an estimation of the critical buckling load as given by Farris (2008). The critical buckling load is relatively accurate for straight girders and mildly curved segments, but the load represents an upper-bound solution for moderately to highly curved segments. For typical steel bridge geometries, mild curvature corresponds to a radius of curvature larger than approximately 548.6 m (1,800 ft), whereas moderate curvature begins around 365.8 m (1,200 ft). The accuracy of the critical buckling load solution decreases as the radius of curvature is decreased. The stress output combines the strong-axis bending, the weak-axis bending, and the warping normal components of stress. The rotational output is the sum of the rigid-body rotation and the cross-sectional twist. In addition, *UT Lift* provides three graphic outputs: (1) the out-of-plane displacements of the top and bottom flanges relative to the girder's original vertical position as a function of the length along the girder, (2) the total rotational deformations of the girder along its length, and (3) the torsion diagram of the girder in the lifted state. The torsion diagram accounts for the effects of cross frames on the girder torque. The position of the cross frames can have a significant effect on the rigid-body rotation, and an engineer may consider positioning them in such a way as to minimize the rigid-body rotation, which *UT Lift* allows a user to do efficiently. For example, an engineer may decide to include only cross frames on the inside arc of the curved girder to reduce the rigid-body motion.

UT Lift Verification

The *UT Lift* program was verified with 3D nonlinear finite-element analyses conducted using *ANSYS*. The graphs presented in Figs. 9–12 compare the centerline rotation from the *ANSYS* analysis with the predicted results from *UT Lift*. Comparisons for both prismatic and nonprismatic girders were made. Figs. 9 and 10 show results for girders with a top flange width-to-depth ratio equal to the TxDOT preferred practice minimum ($b_f/D = 0.33$). The *ANSYS*-calculated rotation is matched almost perfectly by *UT Lift*. Figs. 11 and 12 provide results for girders with a smaller top flange width-to-depth ratio equal to the AASHTO minimum ($b_f/D = 0.167$). The results computed using *UT Lift* compare well with the *ANSYS* results, although there is some discrepancy in the results for extremely flexible girders where second-order effects can become significant. It was noted in all analyses that the *UT Lift* solution closely matched the

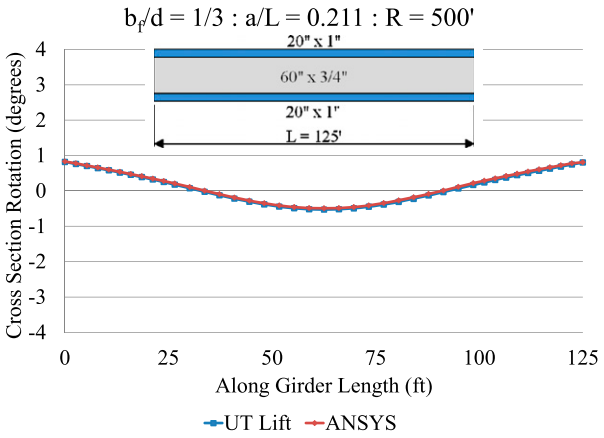

Fig. 9. *UT Lift* verification of prismatic girder

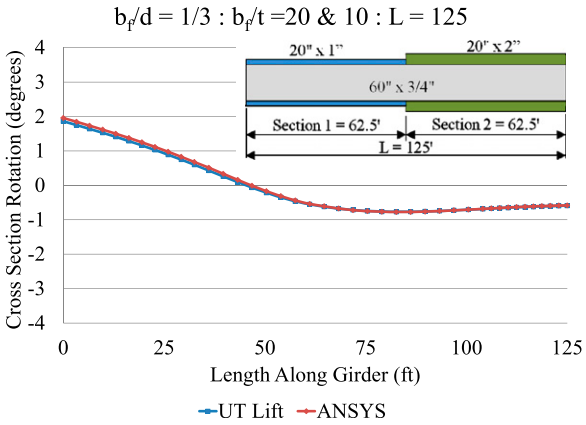

Fig. 10. *UT Lift* verification of nonprismatic girder

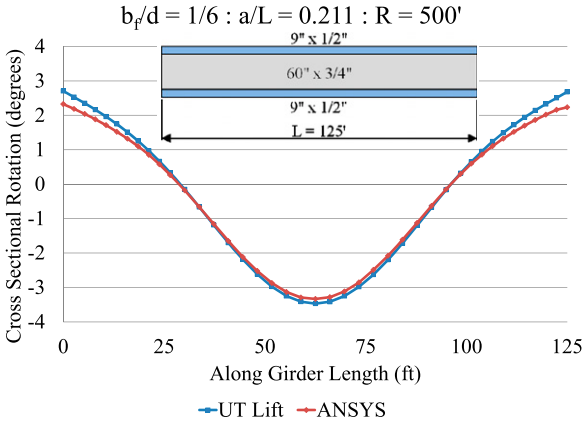

Fig. 11. *UT Lift* verification of prismatic girder

J. Struct. Eng., 2013, 139(4): 481-490

response computed using the *ANSYS* models, with larger errors observed for girders with large initial rigid-body rotations and/or small flange widths. Because the large rotations can render girder segments extremely difficult to splice together, the discrepancies for the cases with very large deformations are not considered to be important because most erectors will develop a different lifting scenario once they are aware of the behavior. A rotation of 1.5° is recommended by the researchers on this study based on feedback from erection and construction personnel (Farris 2008).

Conclusions and Summary

A detailed 3D finite-element model of a girder lift test was created using *ANSYS*, and the collected test data allowed the finite-element model to be verified. Once the computer model was verified, a parametric study was undertaken, and two guidelines for ensuring safety during girder erection were developed based on strength and serviceability limit states. The strength limits should include buckling considerations as well as stress calculations that account for strong-axis bending, weak-axis bending, and warping stresses. For strength limit states, a limiting girder stress should be selected that reflects the effects of residual stresses in the girders as well as the construction-induced stresses during girder erection. In the study reported in this paper, a limit of 50% of the yield stress F_y was considered reasonable based on the potential residual stresses that can exist in a given section. The serviceability limit during erection should consider end rotation at girder splices, and a value of 1.5° is recommended based on results from a national survey of contractors, inspectors, and engineers who specialize in curved steel I-girder systems. The serviceability limit state should account for both the rigid-body rotation and the cross-sectional twist resulting from the torsional self-weight load. The rigid-body rotation depends only on the girder geometry and is not a function of the torsional stiffness. A derivation of a method to numerically determine the torque at any point along a circularly curved nonprismatic girder was derived as a necessary parameter for analyzing the lifting behavior of curved I-girders. The required strength and serviceability limit-state checks can be made quickly and accurately using the *UT Lift* spreadsheet analysis tool. The development of this tool, along with its underlying assumptions, is described in detail in this paper. *UT Lift* has been verified as accurate for cases where the total rotation is limited to reasonable values. *UT Lift*'s linear approximation of the cross-sectional twist deviates from the actual behavior for very flexible girders or girders with large initial rigid-body rotations, but the derived method and tool still provide reasonable estimates of girder deformations even for girder geometries at the AASHTO minimum limits. The University of Texas and TxDOT have made the spreadsheet *UT Lift* available to the public for no charge through the Ferguson Structural Engineering Laboratory website. With this tool, bridge or erection engineers can quickly determine whether girder performance limit states will be satisfied for a given lifting sequence and adjust the lifting scenario as necessary. Such information is crucial for the safe construction of curved I-girders.

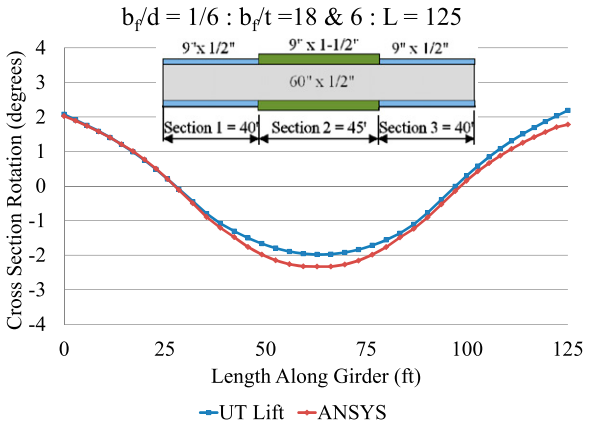

Fig. 12. *UT Lift* verification of nonprismatic girder

Appendix. *UT Lift* Example

An example of the capabilities of *UT Lift* is given for the case of a two-span bridge with skewed supports and varying cross-frame locations. The girder under consideration is positioned over the middle pier, and it has three cross sections and 13 cross-frame locations. Fig. 13 shows a plan view of the bridge, and Fig. 14 gives an elevation view of the girder with a radius of curvature of 365.8 m (1,200 ft).

UT Lift calculates that if the first lift-point location is 9.586 m (31.45 ft) from the beginning and a 23.497-m (77.09-ft) spreader bar is used, the girder will not have any rigid-body rotation. However, because of practical constraints, it would be reasonable to assume that a spreader bar of 22.86 m (75 ft) is used for the lifting. The program then calculates an initial rigid-body rotation for such a spreader bar to be 0.33°. The spreadsheet macro then can be run and the total rotation calculated. The maximum predicted rotation of 0.77° is given at the beginning of the girder, and a maximum stress of 9.86 MPa is given at the first lift point. While the predicted buckling capacity is overpredicted for curved girders using an eigenvalue analysis, it is instructive to note that the predicted buckling capacity is 4.98 MN-m (3,673 k-ft), and the maximum factored moment is 427.1 kN-m (315 k-ft), which is only one-tenth the predicted capacity, thereby indicating a relatively stable girder. *UT Lift* provides three graphic outputs: (1) the out-of-plane displacements of the top and bottom flanges relative to the girder's original vertical position as a function of the length along the girder, (2) the total rotational deformations of the girder along its length, and (3) the torsion diagram of the girder in the lifted state. Figs. 15, 16, and 17,

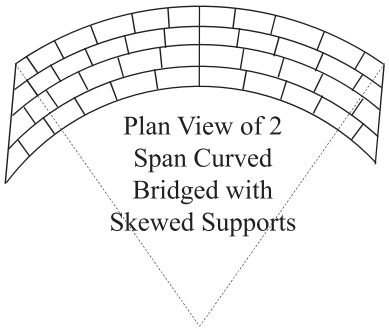

Fig. 13. Plan view of a two-span bridge with skewed supports

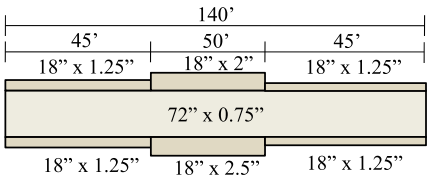

Fig. 14. Elevation view of a girder

J. Struct. Eng., 2013, 139(4): 481-490

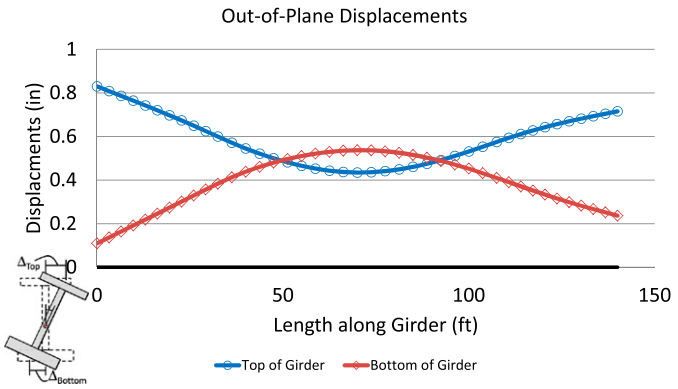

Fig. 15. Out-of-plane displacements of the girder

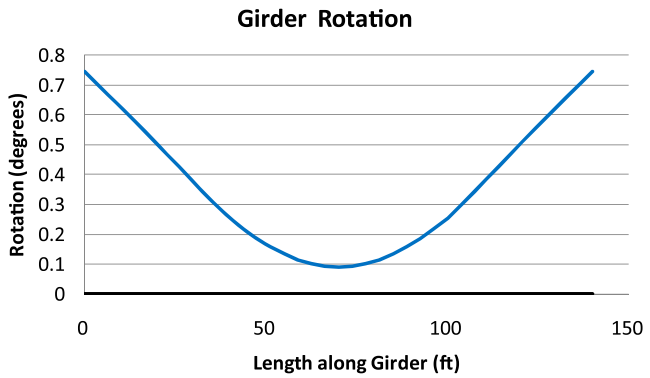

Fig. 16. Total rotations of the girder

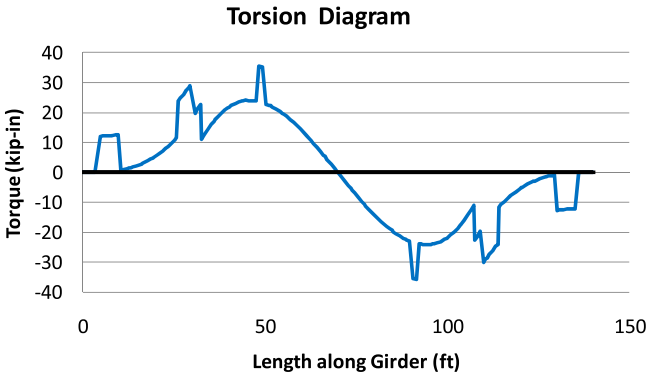

Fig. 17. Torsion diagram of the girder

respectively, are the three graphic outputs for this girder. The sharp changes in the torque at locations along the length represent regions where a cross frame is positioned.

Acknowledgments

The authors acknowledge the Texas Department of Transportation (TxDOT) for its technical and financial support of this project. Additionally, the authors extend their thanks to Hirschfeld Steel Corporation for the use of its facilities and equipment to conduct the field study. The opinions expressed in this paper are those of the authors and do not necessarily reflect those of the sponsors.

Notation

The following symbols are used in this paper:

α = 0 if cross frames are only on both sides of the girder; 1 if cross frames are only on the outside of the curved girder;
$\overline{D}$ = radial distance to center of gravity;
e = eccentricity between center of gravity and the line of support;
$e_{\text{C.G.}i}$ = eccentricity of the center of gravity at cross section i to the line of support;
$e_{\text{S.C.}j}$ = eccentricity of the shear center at cross section j to the line of support;
e_{YOj-i} = eccentricity of the shear center at cross section j to center of gravity at cross section i
H = height of axis of rotation above the top flange;
$\overline{H}_{\text{C.G.}}$ = average girder center-of-gravity location below the top flange;
i = number of cross sections;
j = number of cross frames;
$[K_e]$ = exact torsional stiffness matrix;
$\overline{L}$ = length along girder to center of gravity;
$L_{\text{lift 1}}$ = length along girder to lift point 1;
$L_{\text{lift 2}}$ = length along girder to lift point 2;
$\{Ni(z)\}$ = torsional shape functions;
R = radius of curvature;
s = cross-frame width or spacing of the girders (-1 if cross frames are only on the inside of the curve);
$\{T\}$ = nodal twisting moment;
$\{T_{eFE}\}$ = exact fixed end twisting moment;
t_T = thickness of the top flange;
$t(z)$ = applied distributed twisting moment;
W_i = weight per unit length of cross section i;
W_{xj} = weight of cross frame j;
α = 0 if cross frames are only on both sides of the girder; 1 if cross frames are only on the outside of the curved girder;
θ' = angular distance from lift points to center of gravity;
$\overline{\theta}$ = angular distance to center of gravity;
θ_i = internal angle from the beginning of the girder to the end of section i;
$\theta_{\text{lift 1}}$ = angular distance to lift point 1;
θx_j = internal angle from the beginning of the girder to cross frame j; and
θ_0 = 0; and
$\{\varphi\}$ = nodal rotations.

References

AASHTO. (2010). *AASHTO LRFD bridge design specifications*, 5th Ed., AASHTO, Washington, DC.

ANSYS 11.0 [Computer Software]. Canonsburg, PA, ANSYS.

Beal, D. B., and Kissane, R. J. (1971a). *First Interim Rep. on Research Project 42-1*, New York State Department of Transportation, Engineering Research and Development Bureau, Albany, NY.

Beal, D. B., and Kissane, R. J. (1971b). *Second Interim Rep. on Research Project 42-1*, New York State Dept. of Transportation, Engineering Research and Development Bureau, Albany, NY.
Beal, D. B., and Kissane, R. J. (1972). *Third Interim Rep. on Research Project 42-1*, New York State Dept. of Transportation, Engineering Research and Development Bureau, Albany, NY.
Davidson, J. S. (1996). "Nominal bending and shear strength of curved steel I-girder bridges," Ph.D. dissertation, Auburn Univ., Auburn, AL.
Farris, J. F. (2008) "Behavior of horizontally curved steel I-girders during construction," M.Sc. thesis, Univ. of Texas, Austin, TX ⟨http://fsel.engr.utexas.edu/publications/detail.cfm?pubid=519094101⟩.
Galambos, T. V., Hajjar, J. F., Huang, W., Pulver, B. E., Leon, R. T., and Rudie, B. J. (2000). "Comparison of measured and computed stresses in a steel curved girder bridge." *J. Bridge Eng.*, 5(3), 191–199.
Linzell, D., Leon, R. T., and Zureick, A. (2004). "Experimental and analytical studies of horizontally curved steel I-girder bridge during erection." *J. Bridge Eng.*, 9(6), 521–530.
Mast, R. F. (1989). "Lateral stability of long precast concrete beams." *PCI J.*, 34(1), 34–53.
Mohareb, M., and Nowzartash, F. (2003). "Exact finite element for non-uniform torsion of open sections." *J. Struct. Eng.*, 129(2), 215–223.
Petruzzi, B. J. (2010). "Behavior of horizontally curved steel I-girders during construction," M.Sc. thesis, Univ. of Texas, Austin, TX ⟨http://repositories.lib.utexas.edu/bitstream/handle/2152/ETD-UT-2010-05-1364/PETRUZZI-THESIS.pdf?sequence=1⟩.
Schuh, A. C. (2008). "Behavior of horizontally curved steel I-girders during lifting," M.Sc. thesis, Univ. of Texas–Austin, Austin, TX ⟨http://fsel.engr.utexas.edu/publications/detail.cfm?pubid=211123017⟩.
Stith, J. C. (2010) "Predicting the behavior of horizontally curved I-girders during construction." Ph.D. dissertation, Univ. of Texas, Austin, TX ⟨http://fsel.engr.utexas.edu/publications/detail.cfm?pubid=903120500⟩.
Stith, J. C., et al. (2009). "A method to calculate rotational deformations of curved plate girders during lifting." *Proc., 2009 ASCE Structures Congress*, ASCE, Reston, VA, 68–77.
Stith, J. C., et al. (2012). "Comparisons of the computed and measured behavior of curved steel I-girders during lifting." *J. Struct. Eng.*, 138(1), 1–10.
Texas Department of Transportation (TxDOT). (2007). *Preferred practices for steel bridge design, fabrication, and erection*, Texas Steel Quality Council, Austin, TX.
UT Lift 1.2 [Computer software]. Austin, TX, University of Texas.